PHYSICAL REVIEW E **82**, 060401(R) (2010)

# Enhanced shear separation for chiral magnetic colloidal aggregates

C. I. Mendoza,[1,2] C. M. Marques,[2] and F. Thalmann[2,*]

[1]*Instituto de Investigaciones en Materiales, Universidad Nacional Autónoma de México, Apdo. Postal 70-360, 04510 México, Distrito Federal, Mexico*

[2]*Institut Charles Sadron, Université de Strasbourg, CNRS UPR 22, 23 rue du Loess, Strasbourg Cedex F-67037, France*

(Received 29 March 2010; revised manuscript received 4 November 2010; published 2 December 2010)

We study the designing principles of the simplest colloidal propeller, an architecture built from four identical spheres that can couple translation with rotation to produce controlled drift motion. By considering superparamagnetic beads, we show that the simultaneous action of a magnetic field and a shear flow leads to the migration of the cluster in the vorticity direction. We investigate the dependence of the migration velocity on the geometrical parameters of the cluster and find that significant cluster separation can be achieved under the typical operation conditions of microfluidic devices.

DOI: 10.1103/PhysRevE.82.060401 PACS number(s): 82.70.Dd, 47.57.ef, 85.70.Rp

The motion and the propulsion of microscopic living organisms, the development of top-down techniques to carve micrometer-size devices such as pumps, switches, and motors, the supramolecular chemistry quest for molecular motors, and the new bottom-up techniques that emerge from the soft nanosciences have lead to a reborn interest for the hydrodynamics at low Reynolds numbers Re. In the microscopic world of fluids where typical dimensions $\ell$ are of the order of, or smaller than a few micrometers, $\ell \lesssim 10$ $\mu$m, where the velocities $v$ are smaller than a few micrometers per second, $v \lesssim 10$ $\mu$m s$^{-1}$, the ratio $\mathrm{Re}=\ell v \rho/\eta$ between inertial and viscous forces is extremely small, $\mathrm{Re} \lesssim 10^{-4}$. At these scales, inertia is irrelevant: for all practical purposes when the applied forces stop, the movement stops. Designing feasible and efficient propulsion devices for low Reynolds numbers is arguably one of the main current scientific challenges in the nanosciences. Inspired by recent progress in the self-assembling small numbers of colloidal particles into aggregates with well defined geometries [1], and motivated by the possibility of manipulating colloidal aggregates of superparamagnetic beads with external magnetic fields [2], we propose and study in this Rapid Communication the simplest feasible colloidal aggregate that will behave as a small propeller, capable of transducing rotation into translation and vice versa.

The propeller effect consists in rotating at constant angular velocity $\omega$ a chiral aggregate around a fixed orientation axis, conventionally named $z$, and subsequently referred as the vertical axis, causing a net constant drift velocity $v_z$ along $z$. The propeller efficiency of an aggregate of size $L$ can be expressed as a dimensionless *pitch* $P_p=2\pi v_z/(L\omega)$ that, in the Stokes flow approximation, provides a size independent characterization of its ability to couple rotational and translational motions. Spatial preorientation of the aggregate is required to observe a sizeable linear propeller effect, otherwise strongly suppressed by the free rotational Brownian motion. We show below that this can be achieved with a constant uniform magnetic field acting on superparamagnetic colloids.

Rotation of the aggregate can, in principle, be enforced by means of circular polarized light [3]. Alternatively, a precessing magnetic field with small but finite tilt angle $\beta$ could also be used, but only with low efficiency (i.e., $\sim\beta^2$) [4]. In any case, it is simpler to rely on flows to rotate the clusters, leading naturally to a shear induced vertical drift in Couette geometry.

It was recognized some time ago that the migration under shear flow of a colloidal cluster with randomized orientation only shows a cubic dependence in the shear rate $\dot{\gamma}$ [5]. Shear separation becomes linear in $\dot{\gamma}$ as soon as aggregates get preoriented with respect to the shear flow, with $z$ parallel to the vorticity direction. We introduce the shear separation efficiency ratio $P_s=-4\pi v_z/(L\dot{\gamma})$ as a counterpart of $P_p$, based on a correspondence $\omega=-\dot{\gamma}/2$ between angular velocity and shear rate. Propeller and shear separation are related but were found inequivalent in the cases investigated so far, and comparing $P_p$ and $P_s$ is an important issue. Strong constant shear rates can be experimentally applied, e.g., using soft lithography microfluidic devices [6,7] and shear separation has the potential to become a method of choice for partitioning aggregates according to their chirality.

We first discuss the preorientation of the colloid aggregates by the applied field. Each superparamagnetic bead $i$ making up the aggregate acquires an induced magnetic moment $\vec{m}_i$ and the equilibrium position of the aggregate is the one minimizing the sum $-\Sigma_i \vec{m}_i \cdot \vec{B}/2$, where $\vec{B}$ stands for the uniform gradientless magnetic induction in the absence of colloids. We also assume that the magnetic content of the beads is homogeneous and that the aggregate is rigid. The actual determination of the best orientation of the aggregate depends on the strength of mutual magnetic moments interaction, controlled by a dimensionless parameter $\varepsilon=\mu_0\alpha_b/(32\pi a^3)$, with $\mu_0$ is the permeability, $\alpha_b$ is the magnetic polarizability, i.e., the ratio between magnetization $m$ and induction $B$, and $a$ is the radius of the beads. Provided that (i) the applied magnetic field $\|\vec{B}\|$ is less than a critical value $B_c$ and does not bring $\vec{m}_i$ close to its saturation value, (ii) the time variations of $\vec{B}$ are slower than the Néel relaxation time $\tau_N$ of the magnetic particles, and (iii) the interaction parameter $\varepsilon$ remains smaller than unity, then the magnetic energy reduces to $E_m(\vec{B},\Omega)=\Sigma_{i<j}^n V_{ij}$ with a dipole-

*fabrice.thalmann@ics-cnrs.unistra.fr

 

dipole interaction equal to $V_{ij}=8\alpha_b a^3 \varepsilon \vec{B}^2 r_{ij}^{-3}(1-3\cos^2\theta_{ij})$, $\theta_{ij}$ is the angle between the magnetic field and the vector $\vec{r}_{ij}$ connecting beads $i$ and $j$, and $\Omega$ is a set of Euler angles fixing the orientation of the cluster. This dipolar energy is the leading term of an expansion in powers of $\varepsilon$ that fully takes into account the magnetic interactions between beads.

The quadratic dependence of $E_m(\vec{B},\Omega)$ in $\vec{B}$ at fixed $\Omega$ leads to a unique optimal orientation of the aggregate with respect to $\vec{B}$ if the spectrum of the quadratic form has a single lowest eigenvalue, which is the case for generic nonsymmetric aggregates. Otherwise there may be a degenerate subspace of low-energy configurations, while aggregates with high symmetry end up being totally insensitive to the applied field, as it happens, e.g., for a regular four beads tetrahedron.

For dimers, the preferred orientation is along the field direction; for trimers, as for any planar aggregate, the plane of symmetry of the cluster contains the field direction. These are particular instances of more general orientation rules which are strongly constrained by the symmetry properties of the aggregate. Assuming that a given aggregate possesses a well-defined orientation, then any symmetry plane $\sigma$ of the aggregate is either normal to $\vec{B}$ or contains it, any rotation axis $C_n$ of order $n\geq 3$ is parallel to $\vec{B}$, and any rotation axis $C_2$ ends up being parallel or orthogonal to $\vec{B}$. We assume from now on that our colloidal aggregates possess a well-defined orientation axis and rotate around it. In the case of shear induced migration, the vorticity of the shear flow should be aligned parallel with $\vec{B}$ in order to facilitate the rotation of the aggregate. Flows with vorticity perpendicular to $\vec{B}$ induce torques working against the magnetic stability of the aggregate, ending up with no or little rotation, and are not considered further in the present approach.

Let us consider the linear relation $v_z=\kappa\omega$ between drift and angular velocities of an aggregate with constrained rotation axis $z$. If an inversion center of the aggregate exists, this inversion symmetry preserve both $\kappa$ and $\omega$ while reversing $v_z$. If a mirror symmetry plane containing the axis $z$ exists, it preserves $\kappa$ and $v_z$, but reverses $\omega$. If the mirror plane is orthogonal to the $z$ direction, it preserves $\kappa$ and $\omega$, and reverses $v_z$. Therefore, $\kappa$ vanishes for all nonchiral aggregates. The same consideration holds when a torque $\mathcal{T}$ is applied instead of a constant angular velocity $\omega$. Dimers and trimers are *de facto* ruled out as they possess a mirror plane containing the field. It requires at least four beads to build a propelling aggregate, the only point-symmetry groups allowed for propelling aggregates are, according to Schoenflies terminology, $C_1$, $C_n$, and $D_n$ $(n\geq 2)$ [8].

We will now show that some tetrameric assemblies display indeed propeller and shear separation properties and compute the magnitude of these effects. We consider an aggregate of four identical beads rigidly connected, as depicted in Fig. 1(a). In this configuration, bead one and bead two at a diameter distance $L=2a$ define the main axis. The third bead, connected to bead one defines a lower arm of length $L$ perpendicular to the main axis, and the fourth bead, connected to bead number two defines an upper arm of length $L$, also perpendicular to the main axis. The upper and lower arms are separated by an angle $\delta$. Aggregates with angles $\delta$ and $-\delta$ only differ in their chirality, also called enantiomers. We consider $L$ as the characteristic size of the aggregate.

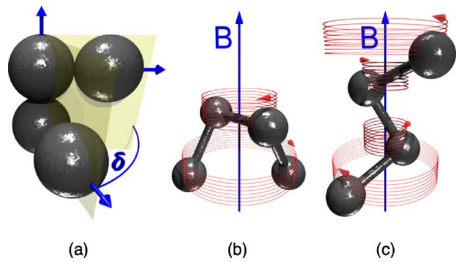


FIG. 1. (Color online) Sketch of the colloidal propeller made of identical superparamagnetic beads. For displaying purposes only, the beads are represented by spheres of a diameter smaller that the arm length in (b) and (c). (a) The propeller consists of a main axis and two perpendicular arms that form an angle $\delta$. For small values of $\delta$, one stable equilibrium position under vertical magnetic field, that we name $\Lambda$ orientation, is shown in (b), the other being obtained by a rotation of 180° around the main axis. For larger values of $\delta$ the equilibrium position that we name $\Sigma$ orientation is shown in (c).

The equilibrium position of such cluster under magnetic field depends on $\delta$. For small values $\delta<\delta_c$, the typical orientation of the cluster that we name orientation $\Lambda$ is displayed in Fig. 1(b). One observes that the field direction is along the (unique) axis of symmetry $C_2$ of the tetramer. For larger values of $\delta$, the stable configuration that we call orientation $\Sigma$ adopts an helical conformation as shown in Fig. 1(c), with $\vec{B}$ perpendicular to the $C_2$ axis, in accordance with the above orientation rules. The $\Lambda$-$\Sigma$ stability exchange caused by an eigenvalues crossing of $E_m(\vec{B},\Omega)$ takes place around $\delta_c\simeq 66.4°$.

Within the Rotne-Prager-Yamakawa dipolar approximation [9] the velocity of the particle located at $\mathbf{R}_m$ is given by the hydrodynamic relation $\mathbf{V}_m=\Sigma_n \mathbf{H}_{mn}\cdot\mathbf{F}_n$, where $\mathbf{F}_n$ are the forces acting on particles and the mobility matrix $\mathbf{H}_{mn}$ is approximated by $\mathbf{H}_{nn}=\mathbf{I}/(6\pi\eta a)$ and $\mathbf{H}_{mn}=\mathbf{H}(\mathbf{R}_m-\mathbf{R}_n)$ for $m\neq n$ with $\mathbf{H}(\mathbf{r})=1/(8\pi\eta r^3)[r^2\mathbf{1}+\mathbf{rr}+2a^2(\mathbf{1}/3-\mathbf{rr}/r^2)]$. The validity of such modeling of cluster hydrodynamics was investigated in [11] and suggests an accuracy within 30% for the rotational drag coefficient. The rigid cluster movement is reducible to three translational and three rotational degrees of freedom collectively denoted as $\mathcal{Q}_\alpha$, $\alpha=x,y,z,\phi,\theta,\psi$, to which are associated generalized forces and torques $\mathcal{F}_\alpha$. Internal constraints can be eliminated by suitably projecting the inverse hydrodynamic tensor $\mathbf{H}^{-1}$ over the collective displacements $\partial\mathbf{R}_m/\partial Q_\alpha$, leading to [10]

$$\dot{Q}_\alpha=\sum_{\gamma=1,\ldots,6}\mathbf{h}^{(6)}_{\alpha,\gamma}\mathcal{F}_\gamma+\mathcal{U}_\alpha, \tag{1}$$

where $\mathbf{h}^{(6)}_{\alpha,\gamma}$ is a $6\times 6$ symmetric mobility matrix restricted to the collective coordinates obeying $(\mathbf{h}^{-1})_{ab}=\Sigma_{m,n}\partial\mathbf{R}_n/\partial Q_a\cdot(\mathbf{H}^{-1})_{nm}\cdot\partial\mathbf{R}_m/\partial Q_b$, $\mathcal{F}_\gamma$ are the external forces and torques components, and $\mathcal{U}_\alpha$ is the generalized components of the streaming flow. In the ideal propeller case, the motion reduces to only two coordinates $\theta$ and $z$, standing, respectively, for the rotation around $z$ axis, and

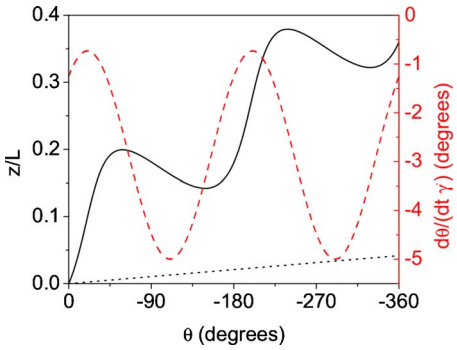


FIG. 2. (Color online) Angular velocity (red dashed line and right vertical axis) and vertical position of the center of mass (black full line and left vertical axis) of the propeller as a function of time while it turns in a shear flow. The straight dotted line represent the vertical motion of a propeller rotating with same angular velocity, $\delta=40°$.

translation parallel to it. In the absence of flow, one gets

$$\dot{z} = \mathbf{h}^{(2)}_{z,z} F_z + \mathbf{h}^{(2)}_{z,\theta} \mathcal{T}_\theta, \quad \dot{\theta} = \mathbf{h}^{(2)}_{\theta,z} F_z + \mathbf{h}^{(2)}_{\theta,\theta} \mathcal{T}_\theta, \tag{2}$$

with $F_z$ is the force, $\mathcal{T}_\theta$ is the torque, and $\mathbf{h}^{(2)}$ is a $2\times2$ symmetric matrix. Equation (2) suffices to discuss the properties of propeller configurations, while Eq. (1) must be numerically integrated when considering shear separation experiments or rotation under precessing magnetic field. Numerical integration of these equations by a fourth-order Runge-Kutta method [12] provides complete solutions for the time evolution of the center of mass and orientation of the propeller.

Applying a torque $\mathcal{T}_\theta$ and no force $F_z$ results in an helical trajectory $\theta(t)$, $z(t)$ associated with a pitch $P_p=(2\pi/L)\dot{z}/\dot{\theta}=(2\pi/L)\mathbf{h}^{(2)}_{\theta,z}/\mathbf{h}^{(2)}_{\theta,\theta}$ which confirms the geometrical, time-reparametrization invariant nature of the motion. In a Couette flow with vorticity parallel to the magnetic field, the aggregate rotates producing an oscillatory vertical movement with a net macroscopic migration along the vorticity direction. The angular velocity of the propeller also oscillates in time, as shown in Fig. 2, depending on the relative attitude of the cluster with respect to the anisotropic shear flow. Curiously enough, the faster vertical motion coincide with the slowest angular velocity part of the trajectory. This can be understood if one observe that an anisotropic shear flow can exert a lift force on a nonrotating aggregate.

We show $P_p$ as a function of $\delta$ in Fig. 3. For the two points with no chirality ($\delta=0°$ and $180°$) the pitch vanishes as expected. $P_p$ is also seen numerically to vanish around $\delta_d\simeq95°$, thus separating the $\Sigma$ regime in two regions with pitches of opposite sign. A maximum of $P_p\simeq0.05$ corresponds to $\delta_c\simeq66°$ and a minimum of $P_p\simeq-0.05$ obtained for $\delta_m\simeq130°$. As a complete rotation of the cluster corresponds to a vertical shift of $\Delta z=P_pL$, it requires about 20 rotations of our cluster to move upwards over its own size.

The shear flow pitch $P_s$ correlates well with $P_p$ in the $\Lambda$ orientation but has a sign opposite to $P_p$ in the $\Sigma$ orientation. In particular, $P_s$ and $P_p$ apparently vanish for the same value $\delta_d$, in agreement with a general argument stating that $P_p=0\Rightarrow P_s=0$, without reciprocity [4]. The propeller efficiency in the absence of external flow is overall lesser than the shear flow efficiency in $\Lambda$ orientation while it is stronger in $\Sigma$ orientation. The relative sign of the two effects depends on the details of the colloidal cluster.

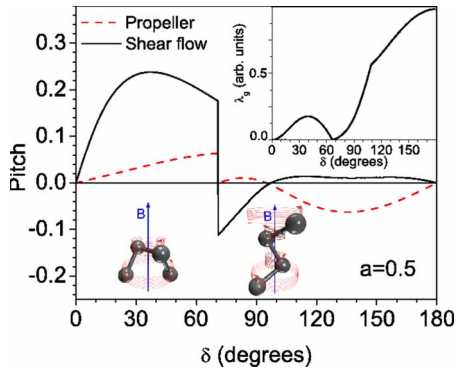


FIG. 3. (Color online) Pitches $P_s$ (shear flow, full black line) and $P_p$ (propeller, dashed red curve) as a function of the angle $\delta$ for touching beads $L=2a$. $\Lambda$ and $\Sigma$ orientations are depicted on the graph, separated by a critical value $\delta_c$. Inset: stability $\lambda_g$ of the magnetically oriented aggregate.

The inset of Fig. 3 shows the stability $\lambda_g(\delta)$ of the magnetic field induced orientation of the cluster, as a function of $\delta$. $\lambda_g$ is defined as twice the difference between the two smallest eigenvalues of the quadratic form $E_m(\vec{B},\Omega)$, with $8\alpha_b\varepsilon=1$. As a result, the depth of the magnetic induced energy minimum and the maximal equilibrium restoring magnetic torque can both be expressed as $\mathcal{E}_{\rm mag}=\mathcal{T}_{\rm mag}=4\varepsilon\alpha_b\lambda_g\vec{B}^2$.

We have so far neglected thermal forces in our analysis. The competition between drift and diffusion defines a Peclet number $\mathrm{Pe}=|v_z|L/D_t$, with a diffusion coefficient $D_t=k_BT/(6\pi\eta L)$. In the sheared situation $v_z=-P_s\dot{\gamma}L/4\pi$ and the ratio between vertical and Brownian displacements scales as $(\dot{\gamma}\,\mathrm{Pe}\,P_st/8\pi)^{1/2}$, defining a characteristic time $t_c=8\pi/(\dot{\gamma}\,\mathrm{Pe}\,P_s)$ beyond which the drift displacement dominates.

Let us illustrate with numbers these phenomena in the case of a shear experiment. Many common superparamagnetic beads contain crystallites of $\gamma Fe_2O_3$ with estimated radius $r_c\simeq10$ nm [13]. Each one of these magnetic grains bears a thermally fluctuating moment of magnitude $m_p=1.9\times10^{-18}$ A m$^2$ with random orientation. This sets the saturation field to $B_c=k_BT/m_p\sim2.2$ mT and the linear response polarizability of crystallites amount to $\alpha_p\sim3\times10^{-16}$ A m$^2$ T$^{-1}$. The Néel relaxation time was experimentally found close to $\tau_N\sim4\times10^{-5}$ s [14]. The polarizability $\alpha_b$ and coupling parameter $\varepsilon$ of a bead both depend on the magnetic material volume fraction $\Phi$, leading, respectively, to $\alpha_b=\alpha_p(a^3/r_c^3)\Phi$ and $\varepsilon\simeq3.6\Phi$.

The dipolar energy used in our approach is correct for the moderately magnetic beads ($\Phi=0.02$, $\varepsilon\simeq0.07$) used in [15] while corrections to the magnetic energy are required for the stronger magnetic beads ($\Phi\simeq0.6$, $\varepsilon\simeq2.2$) studied in [14]. The magnetic orientation energy must exceed the thermal energy $k_BT$. Our calculation is restricted to the linear polarization regime, leading to a magnetic stabilizing energy of

order $\mathcal{E}_{mag} \sim 4.8 \times 10^6 a^3 \Phi^2 \lambda_g k_B T$, with $a$ expressed in micrometers. The magnetic torque $\mathcal{T}_{mag}$ must match the viscous torque $\mathcal{T}_{drag} \sim 4\pi\eta L^3 \dot{\gamma}$ exerted by the flow, with a dynamic viscosity $\eta = 10^{-3}$ Pa s in the case of dilute water solutions. This, at room temperature, limits the shear rate to $\dot{\gamma}_{max} \sim 2.0 \times 10^5 \Phi^2 \lambda_g$ irrespective of cluster size $L$. The larger drift velocity $v_z$ consistent with these constraints scales as $V_{max} = P_s L \dot{\gamma}_{max}/(4\pi)$ or equivalently $V_{max} = 3.1 \times 10^4 P_s a \Phi^2 \lambda_g$, with a corresponding Pe scaling as $\mathrm{Pe} = 5.6 \times 10^5 P_s a^3 \Phi^2 \lambda_g$ ($a$ in micrometers).

For micron sized beads with moderate content in magnetic material ($\Phi = 0.28$), assembled with an angle $\delta = 40°$, one reads from Fig. 3 the values $\lambda_g \sim 0.18$ and $P_s = 0.25$. One obtains a maximal shear rate $\dot{\gamma}_{max} \sim 2800\ \mathrm{s}^{-1}$, a maximal drift velocity $V_{max} = 110\ \mu\mathrm{m\ s}^{-1}$, $t_c = 18\ \mu\mathrm{s}$, and $\mathrm{Pe} = 2000$. This should be fast enough to induce some enantiomer separation using a microfluidic chip like the one described in [6] with a magnetic field aligned parallel to the chip and orthogonal to the main direction of the flow. The scaling $\mathrm{Pe} \sim a^{-3}$ limits our results to sizes $a = 80$ nm below which $\mathrm{Pe} \leq 1$ and Brownian forces cannot be neglected any longer.

In summary, we have applied an hydrodynamic interaction formalism for studying the rotational-translational coupling for a chiral propeller made of four identical beads. This coupling can be optimized by changing the geometry of the aggregate. Chiral superparamagnetic colloidal enantiomers can be oriented and separated under the simultaneous action of a magnetic field and a shear flow even at relatively low shear rates since they migrate in opposite directions with velocity proportional to the applied shear. Propeller and shear separation properties are distinct features, their relative sign may change depending on the details of the cluster and are not simply related to the handedness of the chiral aggregate [16]. Quantitative estimates of the magnitude of this magnetic field assisted drift are given that support the feasibility of the experiment with microfluidic devices.

C.I.M. acknowledges the Chemistry Department of the Centre National de la Recherche Scientifique for a visiting grant and partial financial support by DGAPA-PAPIIT Grant No. IN-115010. Enlightening discussions are acknowledged with Paul Chaikin and Thomas Ebbesen.

[1] V. N. Manoharan, M. T. Elsesser, and D. J. Pine, Science **301**, 483 (2003); D. Zerrouki, *et al.*, Nature **455**, 380 (2008).
[2] R. Dreyfus *et al.*, Nature (London) **437**, 862 (2005).
[3] A. I. Bishop, T. A. Nieminen, N. R. Heckenberg, and H. Rubinsztein-Dunlop, Phys. Rev. Lett. **92**, 198104 (2004).
[4] C. I. Mendoza, C. M. Marques, and F. Thalmann (unpublished).
[5] M. Doi and M. Makino, Prog. Polym. Sci. **30**, 876 (2005); M. Makino and M. Doi, Phys. Fluids **17**, 103605 (2005).
[6] Marcos, H. C. Fu, T. R. Powers, and R. Stocker, Phys. Rev. Lett. **102**, 158103 (2009).
[7] R. Eichhorn, Phys. Rev. Lett. **105**, 034502 (2010).
[8] R. L. Carter, *Molecular Symmetry and Group Theory* (Wiley and Sons, New York, 1998).
[9] J. Rotne and S. Prager J. Chem. Phys., **50**, 4831 (1969); H. Yamakawa, *ibid.* **53**, 436 (1970).
[10] M. Doi and S. F. Edwards, *The Theory of Polymer Dynamics* (Oxford UniversityPress, New York, 2001).
[11] J. García de la Torre, G. del Rio Echenique, and A. Ortega, J. Phys. Chem. B **111**, 955 (2007).
[12] G. Arfken, *Mathematical Methods for Physicist* (Academic Press, London, 1985).
[13] U. Jeong *et al.*, Adv. Mater. **19**, 33 (2007).
[14] P. C. Fannin *et al.*, J. Magn. Magn. Mater. **303**, 147 (2006).
[15] K. Zahn, J. M. Méndez-Alcaraz, and G. Maret, Phys. Rev. Lett. **79**, 175 (1997).
[16] A. B. Harris, R. D. Kamien, and T. C. Lubensky, Rev. Mod. Phys. **71**, 1745 (1999).